

Topological nodal Cooper pairing in doped Weyl metals

Yi Li¹ and F. D. M. Haldane²

¹*Princeton Center for Theoretical Science, Princeton University, Princeton, NJ 08544, USA*

²*Department of Physics, Princeton University, Princeton, NJ 08544, USA*

(Dated: December 10, 2018)

We generalize the concept of Berry connection of the single-electron band structure to the two-particle Cooper pair states between two Fermi surfaces with opposite Chern numbers. Because of underlying Fermi surface topology, the pairing Berry phase acquires non-trivial monopole structure. Consequently, the pairing gap functions have a topologically-protected nodal structure as vortices in momentum space with its total vorticity determined by the monopole charge q_p . The pairing nodes behave as the Weyl-Majorana points of the Bogoliubov-de Gennes pairing Hamiltonian. They determine the connection pattern of the surface modes from the band structure Weyl points and the Majorana surface modes inside the pairing gap. Under the approximation of spherical Fermi surfaces, the pairing symmetry are represented by monopole harmonic functions. The lowest possible pairing channel carries angular momentum number $j = |q_p|$, and the corresponding gap functions are holomorphic or anti-holomorphic functions on Fermi surfaces.

PACS numbers: 74.20.Rp, 73.43.-f, 03.65.Vf

The study of topological states has renewed our understanding of condensed matter physics. The discovery of two-dimensional integer quantum Hall states^{1,2} started the exploration of novel states characterized by band topology rather than symmetry³⁻⁸, whose magnetic band structures possess non-trivial Chern numbers arising from the broken time-reversal (TR) symmetry. For band structures of lattice Bloch-waves, the Berry curvatures led to rich studies of anomalous Hall and quantum anomalous Hall physics⁹⁻¹⁶. The band structure topology has also been generalized to systems of topological insulators with TR symmetry¹⁷⁻²⁸. Similar to the stable gapless surface modes which appear at the boundary of gapped topological systems, gapless semi-metallic systems have also been discovered with non-trivial band topology. For example, topological Weyl semi-metals have been proposed and realized in three-dimensional systems in the absence of either TR or inversion symmetry²⁹⁻⁵⁰. Their band structure is characterized by degenerate Weyl points in the momentum space, which can be effectively understood as the sources and drains of the magnetic monopole flux defined in the momentum space.

Topological phenomena are usually understood as the contribution from all the filled electronic states rather than the states in the vicinity of Fermi surfaces. While, the seeming disagreement with Fermi-liquid theory could be nicely resolved by introducing the Berry phase of quasiparticles near the Fermi surface¹³. So far, the study of the Fermi surface topology and the associated Berry phase structure has mainly been discussed at the single-particle level¹¹⁻¹⁴.

In this article, we study a novel class of exotic superconductivity which can be realized in the doped Weyl metals, and generally in systems with topologically non-trivial Fermi surfaces. For the inter-Fermi surface pairing between two Fermi surfaces with opposite Chern numbers, the Cooper pair inherits a non-trivial Berry struc-

ture from the underlying single-particle Fermi surfaces. Consequently, the pairing gap functions develop nontrivial net vorticities leading to topologically-stable nodes on Fermi surfaces. These nodes also determine the interplay between the surface modes due to the Weyl point of the band structure and those arising from the Cooper pairing. For Fermi surfaces with approximate spherical symmetries, the pairing symmetry can be classified by the monopole harmonic functions rather than ordinary spherical harmonic functions.

We consider a general three-dimensional (3D) electron system with a pair of separated Fermi surfaces, denoted as FS_{\pm} , respectively, carrying opposite Chern numbers $\pm C$. The doped Weyl metal can be thought as a concrete example. Let us start with a minimal description - only assuming the existence of inversion symmetry but broken TR symmetry. No additional crystalline symmetry is imposed. In this model, FS_{\pm} enclose two Weyl points located at $\pm \mathbf{K}_0$ and are related to each other by parity. Further, the parity symmetry ensures opposite monopole charges $\pm q$ carried by FS_{\pm} . Define the electron creation operator $c_a^{\dagger}(\mathbf{k})$ in which a is the index of a general two-band structure. For example, a may refer to the σ_z -eigenvalue in a spin-orbit coupled spin- $\frac{1}{2}$ system, or, a sublattice index in a bipartite lattice with spinless fermions. For the single-electron states on FS_{\pm} , their creation operators are defined, respectively, as

$$\alpha_{\pm}^{\dagger}(\pm \mathbf{k}) = \sum_a \xi_{\pm,a}(\pm \mathbf{k}) c_a^{\dagger}(\pm \mathbf{K}_0 \pm \mathbf{k}), \quad (1)$$

in which $\pm \mathbf{k}$ are the relative momenta for electrons on FS_{\pm} with respect to $\pm \mathbf{K}_0$. $\xi_{\pm,a}(\pm \mathbf{k})$ are the corresponding normalized eigen-functions on FS_{\pm} , respectively. And $\pm \mathbf{k}$ lie on two surfaces denoted as S_{\pm} which correspond to shifting FS_{\pm} by $\mp \mathbf{K}_0$ towards the origin. Because of the non-trivial monopole structure, $\xi_{\pm,a}(\pm \mathbf{k})$ cannot be globally well-defined for $\pm \mathbf{k}$ over the entire surfaces of S_{\pm} , respectively. They need to be presented under a

certain gauge.

The single-particle Berry connection can be defined as $\mathbf{A}_\pm(\mathbf{k}) = \sum_a \xi_{\pm,a}^*(\mathbf{k}) i \nabla_{\mathbf{k}} \xi_{\pm,a}(\mathbf{k})$, in which $\nabla_{\mathbf{k}}$ lies in the tangent space of S_\pm , and thus, \mathbf{A}_\pm is a tangent vector field therein. The Berry fluxes satisfy $\iint_{S_\pm} d\mathbf{k} \cdot \nabla_{\mathbf{k}} \times \mathbf{A}_\pm(\mathbf{k}) = \pm 4\pi q$. The simplest case of $C = 1$ is associated with the fundamental monopole charge of $q = \frac{1}{2}$.

Let us consider the inter-Fermi surface pairing between FS_+ and FS_- , which is a zero momentum pairing. The pairing operator is defined as $P^\dagger(\mathbf{k}) = \alpha_+^\dagger(\mathbf{k}) \alpha_-^\dagger(-\mathbf{k})$. The Berry connection of the two-particle state created by $P^\dagger(\mathbf{k})$ as varying \mathbf{k} on S_+ is calculated as $\mathbf{A}_p(\mathbf{k}) = \mathbf{A}_+(\mathbf{k}) - \mathbf{A}_-(-\mathbf{k})$. The total pairing Berry flux penetrating S_+ is

$$\iint_{S_+} d\mathbf{k} \cdot \nabla_{\mathbf{k}} \times \mathbf{A}_p(\mathbf{k}) = 4\pi q_p, \quad (2)$$

in which $q_p = 2q$. In other words, the inter-Fermi surface Cooper pairing inherits the Berry fluxes of two single-electron Fermi surfaces. Consequently, the Cooper pairing phases cannot be well-defined over the entire Fermi surfaces, which leads to the following theorem.

Consider the gap function defined as $\Delta(\mathbf{k})$, which is conjugate to the pairing operator $P^\dagger(\mathbf{k})$. It is a single-valued complex function defined on S_+ . The nodal structure $\Delta(\mathbf{k})$ is assumed measure zero, or equivalently, composed of isolated points or lines. Under this assumption, we have

Theorem 1 $\Delta(\mathbf{k})$ possesses generic nodal structure with the total vorticity $2q_p$, which is a consequence of the band topology on FS_\pm and is independent of specific pairing mechanisms and symmetries.

Proof: The gap function $\Delta(\mathbf{k})$ can be parameterized as $|\Delta(\mathbf{k})|e^{i\phi(\mathbf{k})}$ in which $\phi(\mathbf{k})$ is the pairing phase. $\Delta(\mathbf{k})$ is gauge-covariant as follows: Under the gauge transformation $\xi_\pm(\pm\mathbf{k}) \rightarrow \xi_\pm(\pm\mathbf{k})e^{i\Lambda_\pm(\pm\mathbf{k})}$, we have $\alpha_\pm^\dagger(\pm\mathbf{k}) \rightarrow \alpha_\pm^\dagger(\pm\mathbf{k})e^{i\Lambda_\pm(\pm\mathbf{k})}$, and $P^\dagger(\mathbf{k}) \rightarrow P^\dagger(\mathbf{k})e^{i\Lambda(\mathbf{k})}$ in which $\Lambda(\mathbf{k}) = \Lambda_+(\mathbf{k}) + \Lambda_-(-\mathbf{k})$. Consequently, $\phi(\mathbf{k})$ and $\mathbf{A}_p(\mathbf{k})$ transform as $\phi(\mathbf{k}) \rightarrow \phi(\mathbf{k}) - \Lambda(\mathbf{k})$, and $\mathbf{A}_p(\mathbf{k}) \rightarrow \mathbf{A}_p(\mathbf{k}) - \nabla_{\mathbf{k}}\Lambda(\mathbf{k})$. We define a gauge invariant tangential vector field, ‘‘velocity’’, on S_+ as $\mathbf{v}(\mathbf{k}) = \nabla_{\mathbf{k}}\phi(\mathbf{k}) - \mathbf{A}_p$, which is regular except at gap nodes. We first consider the case that $\Delta(\mathbf{k})$ only has isolated zeros located at \mathbf{k}_i ($i = 1, 2, \dots, n$). An infinitesimal oriented loop C_i is defined around each zero \mathbf{k}_i whose positive direction depends on the local normal direction by a right-hand rule. Then, $\oint_{C_i} d\mathbf{k} \cdot \mathbf{v} = 2\pi g_i$ in which g_i is the vorticity and integer-valued. Next, reversing the direction of each loop C_i and apply Stokes’ theorem on S_+ excluding the bad points \mathbf{k}_i ’s on which \mathbf{v} is ill-defined, we arrive at

$$\sum_i g_i = \frac{1}{2\pi} \sum_i \oint_{C_i} d\mathbf{k} \cdot \mathbf{v} = \iint \frac{d\mathbf{k}}{2\pi} \cdot (\nabla_{\mathbf{k}} \times \mathbf{A}_p) = 2q_p. \quad (3)$$

This proof is gauge-independent. If $\Delta(\mathbf{k})$ has line-nodes on S_+ which behave as branch-cuts of \mathbf{v} , the proof can also be done similarly. Q.E.D.

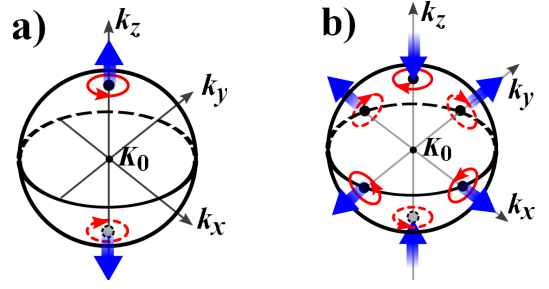


FIG. 1. The vorticity and nodal structure of the pairing gap function $\Delta(\mathbf{k})$ on the bulk Fermi surface S_+ . The total vorticities equal $+2$ according to Theorem 1. The vortices at the north and south poles exhibit the vorticity ± 1 for (a) $\Delta_y = -i\Delta_x$ and (b) $\Delta_y = i\Delta_x$, respectively. Each of the four additional nodes in (b) exhibit the vorticity $+1$.

Remark When $q_p \neq 0$, Theorem 1 states that $\Delta(\mathbf{k})$ cannot be a regular function over the entire surface of S_+ . Its nodal structure is distinct from the familiar examples of pairing symmetries characterized by the spherical harmonic functions $Y_{lm}(\hat{\mathbf{k}})$. $Y_{lm}(\hat{\mathbf{k}})$ is a regular function over the sphere in the absence of the monopole structure, and thus the total vorticity of phases vanishes. For example, for the $^3\text{He-A}$ type pairing with the orbital symmetry $Y_{11}(\hat{\mathbf{k}})$, two gap nodes lie at the north and south poles as a pair of vortex and anti-vortex of the pairing phase field, respectively.

For further illustration, we employ a concrete simple model for the 3D Weyl metal defined in a bipartite lattice with spinless fermions^{40,50} as

$$H_K = \sum_{\mathbf{k}} c_a^\dagger(\mathbf{k}) \left\{ V(k_y) \sigma_3 + [t_- \cos(2k_x) + t_+(k_y, k_z)] \sigma_1 + \sin 2k_x \sigma_2 - \mu \right\} c_b(\mathbf{k}) + h.c., \quad (4)$$

in which the σ_z -eigen basis refer to A and B sublattices; $V_{k_y} = 2k_y$, $t_+(k_y, k_z) = -(k_y^2 + k_z^2)$ and $t_- = 1$. H_K is invariant under the inversion transformation with respect to the center of a bond along x -direction, *i.e.*, $A \leftrightarrow B$, $k_{y,z} \rightarrow -k_{y,z}$, and it breaks TR symmetry. This Hamiltonian gives rise to a pair of Weyl point located at $\pm \mathbf{K}_0 = (0, 0, \pm 1)$ along the z -axis, respectively. If $\mu > 0$, FS_\pm enclosing $\pm \mathbf{K}_0$ possess the Chern number $C = \pm 1$, respectively. For small values of μ , FS_\pm are approximately spheres. Consider the following pairing Hamiltonian,

$$H_\Delta(\mathbf{k}) = \sum_{\mathbf{k}} c^\dagger(\mathbf{k}) (2i\Delta_x \sin 2k_x + 2i\Delta_y \sin k_y \sigma_1) c^\dagger(-\mathbf{k}) + h.c. \quad (5)$$

The lattice constructions of Eqs. (4) and (5) are presented in the Supplemental Material (Suppl. Mat.) A.

Assuming that the system is in the weak pairing region, *i.e.*, $|\Delta_{x,y}| \ll |\mu|$, we can project the pairing to FS_\pm . Since the gap function satisfies the relation $\Delta(-\mathbf{k}) = -\Delta(\mathbf{k})$, we only need to consider $\Delta(\mathbf{k})$ on

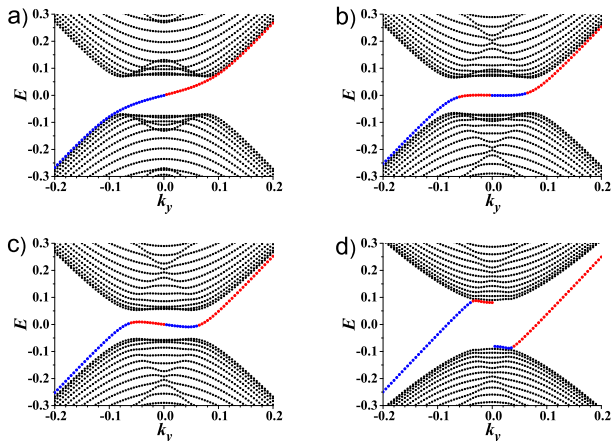


FIG. 2. (Color Online) The bulk spectrum and surface dispersions on one open boundary of the yz -plane v.s. k_y at different cuts of $k_z = 1.03, 0.95, 0.93, 0.85$ from (a) to (d), respectively. The parameters are $\Delta_y = -i\Delta_x$ with $\Delta_x = 0.2$ and $\mu = 0.2$. The cuts of k_z lie between the intersecting points of the z -axis on FS_+ for (a), (b), and (c), while k_z in (d) lies outside FS_+ . The red (blue) color represents the positive (negative) charge carried by the surface modes.

FS_+ . $\Delta(\mathbf{k})$ exhibits two nodes at the north and south poles, respectively. We choose two different gauges, which are non-singular in these two polar regions, respectively. Then, the gap function can be approximated as $\Delta(\mathbf{k}) = \mp\Delta_x k_x + \Delta_y k_y$ at north and south poles, respectively. If $\Delta_y = -i\Delta_x$, the velocity field $\mathbf{v}(\mathbf{k})$ exhibits a pair of vortices located at north and south poles with the vorticity $+1$ as shown in Fig. 1 (a). There are no other nodes on the FS_+ , and the total vorticity is $+2$ in agreement with Theorem 1. In contrast, if $\Delta_y = i\Delta_x$, each of the nodes at the north and south poles changes its vorticity to -1 . To maintain the total vorticity, there appears additional four nodes on FS_+ , each of which exhibits the vorticity of $+1$ as shown in Fig. 1 (b). In our case, their approximate locations are on the equator with azimuthal angles $\pm\frac{\pi}{4}, \pm\frac{3\pi}{4}$.

We have further calculated the surface mode spectra on the open boundary. In the absence of pairing, it is well-known that the chiral surface states appear inside the band gap for k_z lying in the region of $-K_{0,z} < k_z < K_{0,z}$, which connect two bulk Weyl points as shown in Ref. [13]. Cooper pairing opens pairing gap on FS_\pm , and generates additional Majorana surface modes inside the pairing gap. These Majorana surface modes are determined by the pairing nodal structure on FS_\pm and the associated vorticity pattern. Furthermore, these Majorana surface modes connect with those arising from the Weyl band structures as the cut of k_z varies as explained below.

We impose two open boundaries parallel to the yz -plane, and plot the spectra v.s. k_y at different cuts of k_z . The results of the case $\Delta_y = -i\Delta_x$ are shown in Fig. 2 (a)-(d). Under the Bogoliubov-de Gennes (BdG) formalism, the system becomes 4-bands but only states

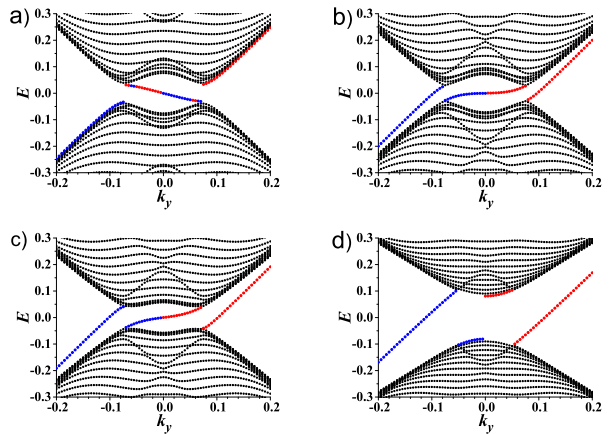


FIG. 3. (Color Online) The bulk spectrum and surface dispersions on one open boundary of the yz -plane v.s. k_y at different cuts of k_z . The parameters and the value of k_z in each subfigure are the same as those in Fig 2 except that $\Delta_y = i\Delta_x$. The chiralities of the Majorana surface modes at k_z close to the north and south poles are opposite to those in the case of $\Delta_y = -i\Delta_x$. The red (blue) color represents the positive (negative) charge carried by the surface modes.

with $k_z > 0$ are independent. At $\mu = 0.2$, FS_+ intersects the z -axis at $k_n \approx 1.1$ (the north pole) and $k_s \approx 0.9$ (the south pole). For the cut of $k_z > k_n$, or, $k_z < k_s$, it does not intersect FS_+ . The corresponding surface spectra are determined by the Weyl band structure: No surface modes exist at $k_z > k_n$, and two branches of chiral surface modes appear at $0 < k_z < k_s$ as shown in Fig. 2 (d). In the BdG formalism, after the particle-hole transformation, the band Weyl point at $-\mathbf{K}_0$ is reflected to \mathbf{K}_0 with flipped chirality and energy $+\mu$. Consequently, at $0 < k_z < k_s$, one branch of surface modes is particle-like, while the other one is the hole version of modes at $k_z < 0$. Because k_z lies outside FS_\pm , the particle-hole mixing are weak. The band structure Weyl points are with the energy $\mp\mu$, both of which are away from the zero energy. The transition of the topological classes at $k_z > k_n$ and at $k_s > k_z > 0$ must occur through gap closings during $k_n > k_z > k_s$. In this region, each k_z cuts a cross section (CS) on FS_+ termed as Fermi-CS below, which are gapped because of pairing except at the nodal points. These points are Majorana-Weyl (M-W) points in the BdG formalism, which are denoted as positive or negative according to their chiral indices. The two M-W points at the north and south poles both carry positive pairing vorticities $+1$. As k_z decreases, passing the M-W point at the north pole, there should first appear only one connected branch of surface modes at $k_n > k > k_s$ as shown in Fig. 2 (a), (b) and (c). After k_z further passes the other M-W point at the south pole which also has pairing vorticity $+1$, the number of the branches of surface modes is increased to 2.

When $k_n > k_z > k_s$, the Majorana surface modes appear inside the pairing gap if k_y is inside the Fermi-CS.

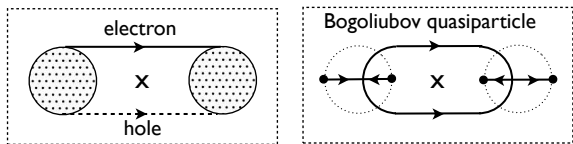


FIG. 4. Comparison of surface states (zero-energy locus) of doped Weyl semimetals in the surface Brillouin zone, without (left panel) and with (right panel) superconductivity. (“X” marks a 2D inversion center.) The directions indicated on the arc are $\hat{\mathbf{n}} \times \hat{\mathbf{v}}$, where $\hat{\mathbf{n}}$ is the normal to the surface, and \mathbf{v} is the group velocity of the surface mode. The “flow” starts and ends at sources and sinks of Berry flux. A “vector central charge” $\tilde{c}\hat{\mathbf{v}}$ with $\tilde{c} = \frac{1}{2}$ is associated with the Bogoliubov edge modes (directed solid lines) in the right panel. In the left panel, the Dirac (Weyl) electron model (solid line with $\tilde{c} = 1$) can be split into a positive-energy charge- e “electron” part at \mathbf{k} , and a positive-energy charge- $(-e)$ “hole” at $-\mathbf{k}$, both with $\tilde{c} = \frac{1}{2}$. In the Bogoliubov case (right), the charge carried by the $\tilde{c} = \frac{1}{2}$ positive-energy modes varies continuously from close to $\pm e$ on the electron-like and hole-like arcs, falling continuously to zero where they coalesce with $\sum \tilde{c}\hat{\mathbf{v}} = 0$, and reemerge as two strictly-zero-charge Majorana arcs.

Actually, their properties change as k_z varies. As k_z decreasing from k_n , the dispersions of the Majorana surface modes become softer, and even flat in Fig. 2 (b). As k_z further goes down from the northern hemisphere to the southern hemisphere in Fig. 2 (c), the chirality of the Majorana modes reverses. This is because the vorticities at the north and south poles are along $\pm z$ -directions, respectively. However, there are no additional nodes in the region of $k_n > k_z > k_s$, thus, the overall chirality of the surface modes should remain the same. To solve this discrepancy, the Majorana surface modes inside the Fermi-CS are found connected to the surface modes from the Weyl band structure outside the Fermi-CS as shown in Fig. 2 (c). The surface mode dispersions are non-monotonic: the velocities outside and inside the Fermi-CS are opposite. The level of particle-hole mixing is strong inside the Fermi-CS but weak outside. The Majorana surface modes disappear as k_z goes below k_s .

The surface spectra at the case of $\Delta_y = i\Delta_x$ are also calculated as presented in Fig. 3. The surface modes in the cases of $k_z > k_n$ and $k_s > k_z > 0$ are not directly related to pairing, and thus are qualitatively the same as the case of $\Delta_y = -i\Delta_x$. However, the Majorana surface modes at $k_n > k_z > k_s$ are markedly different due to the more complicated nodal structure on FS_+ . According to the vorticity structure illustrated in Fig. 1 (b), the M-W points at the north and the south poles are negative; while, those near the equator are positive. As k_z moves downward passing k_n , Majorana surface modes appear inside the pairing gap as in Fig. 3 (a), but its chirality is opposite to that in Fig. 2 (a). Again as k_z moves downward, the dispersions of the Majorana surface modes become softer. Actually after k_z passes the four positive M-W points, the Majorana surface modes

inside the Fermi-CS switches the chirality accompanied by the appearance of two branches of Weyl surface modes outside the Fermi-CS with the same chirality as shown in Fig. 3 (b) and (c). As k_z further passes the south pole, which is a negative M-W point, the Majorana surface modes disappear leaving two branches of Weyl surface modes outside the Fermi-CS.

Next we study the pairing partial-wave symmetries when FS_\pm have an approximate spherical symmetry. If we neglect the small anisotropy, the complete bases of $\Delta(\mathbf{k})$ for \mathbf{k} lying on S_+ with the total vorticity q_p can be spanned by the monopole harmonic functions $Y_{q_p, jm}(\hat{\mathbf{k}})$ instead of the usual Y_{lm} . Monopole harmonic functions have been widely applied in physics^{4,51,52}. For completeness, their basic properties are summarized in Suppl. Mat. B. After projecting the pairing Hamiltonian to FS_\pm , it becomes $H_\Delta = \sum_{\mathbf{k}} \Delta(\mathbf{k})P^\dagger(\mathbf{k}) + \Delta^*(\mathbf{k})P(\mathbf{k})$ for \mathbf{k} lying close to S_+ . We define $\Delta(\mathbf{k}) = \Delta(|k|)f(\hat{\mathbf{k}})$, in which the angular dependence on $\hat{\mathbf{k}}$ and the energy dependence on $|k|$ are separated. $\Delta(|k|)$ is assumed positive and the angular factor $f(\hat{\mathbf{k}})$ is complex satisfying the normalization condition $\int d\hat{\mathbf{k}} |f(\hat{\mathbf{k}})|^2 = 1$. $f(\hat{\mathbf{k}})$ is expanded in terms of the monopole harmonic functions as

$$f(\hat{\mathbf{k}}) = \sum_{jm} c_{jm} \mathcal{Y}_{q_p, jm}(\hat{\mathbf{k}}), \quad (6)$$

in which c_{jm} are complex coefficients. Both the pairing operator $P^\dagger(\mathbf{k})$ and the gap function $\Delta(\mathbf{k})$ are gauge dependent, while, H_Δ is gauge independent.

A remarkable feature is that all the pairing channels should be $j \geq |q_p|$ regardless of the pairing mechanism since $\mathcal{Y}_{q_p, j, m}$ starts with $j = |q_p|$. The absence of pairing channels with $j < |q_p|$ is robust, which is a consequence of topology and the monopole harmonic representation of the rotation group. Furthermore, the lowest order pairing channel $j = |q_p|$ is special: $\mathcal{Y}_{q_p, j=|q_p|, m}(\hat{\mathbf{k}})$ are holomorphic or anti-holomorphic functions. All of its $2q_p$ -nodes exhibit the same vorticity, and thus $\Delta(\mathbf{k})$ is completely determined by the locations of its nodes up to an overall factor. The nodes of $\mathcal{Y}_{q_p, j=|q_p|, m}(\hat{\mathbf{k}})$ represent vortices of the pairing phases on S_+ . The location of pairing nodes are also Weyl-Majorana points of the BdG Hamiltonian with the same chirality. For each node on FS_+ with $\mathbf{K}_0 + \mathbf{k}$, there exists its image on FS_- exhibiting the opposite vorticity.

Let us consider a concrete example of spinful fermions in the continuum with spin-orbit coupling. The low energy kinetic Hamiltonians around the Weyl points are

$$H_{\text{Weyl}, \pm}(\pm \mathbf{K}_0 + \mathbf{k}) = \pm v_F \boldsymbol{\sigma} \cdot \mathbf{k} - \mu, \quad (7)$$

where $\boldsymbol{\sigma}$'s represent Pauli matrices for spin; $\mu > 0$ is assumed without loss of generality. We choose the gauge convention: $\xi_+(\hat{\mathbf{k}}) = \xi_-(-\hat{\mathbf{k}}) = (u_{\hat{\mathbf{k}}}, v_{\hat{\mathbf{k}}})^T$, in which $u_{\hat{\mathbf{k}}} = \cos \frac{\theta_{\hat{\mathbf{k}}}}{2}$ and $v_{\hat{\mathbf{k}}} = \sin \frac{\theta_{\hat{\mathbf{k}}}}{2} e^{i\phi_{\hat{\mathbf{k}}}}$, which are singular when $\hat{\mathbf{k}}$ is located at the north and the south poles on FS_\pm ,

respectively. $P^\dagger(\mathbf{k}) = \alpha_+^\dagger(\mathbf{k})\alpha_-^\dagger(-\mathbf{k})$ is a spin-1 helicity eigen-operator, satisfying $[\mathbf{S} \cdot \hat{\mathbf{k}}, P^\dagger(\mathbf{k})] = P^\dagger(\mathbf{k})$, in which \mathbf{S} is the total spin of the Cooper pair. Under the S_z -eigenbasis, $P^\dagger(\mathbf{k}) = \sum_{m=-1}^1 \sqrt{\frac{4\pi}{3}} \mathcal{Y}_{-1;1m}^*(\hat{\mathbf{k}}) \chi_{1m}^\dagger(\mathbf{k})$, in which $\chi_{1m}^\dagger(\mathbf{k}) = \langle 1m | \frac{1}{2} \sigma_{\frac{1}{2}} \sigma_{\frac{1}{2}}' \rangle c_\sigma^\dagger(\mathbf{K}_0 + \mathbf{k}) c_{\sigma'}^\dagger(-\mathbf{K}_0 - \mathbf{k})$. The monopole charge enclosed by S_+ is $q_p = -1$ for the phase distribution of $\Delta(\mathbf{k})$. According to Eq. (6), by setting $j = |q_p| = 1$, $f(\hat{\mathbf{k}})$ is a quadratic homogeneous function of u_k and v_k^*

$$f(\hat{\mathbf{k}}) = f(u_k, v_k) = \frac{1}{\sqrt{N}} \prod_{i=1,2} (u_k v_i^* - u_i v_k^*), \quad (8)$$

in which N is the normalization factor; the nodal points are represented by $(u_i, v_i)^T = (\cos \frac{\theta_i}{2}, \sin \frac{\theta_i}{2} e^{i\phi_i})^T$ with $i = 1, 2$.

The locations of nodes in $f(\hat{\mathbf{k}})$ are determined by the energetics which can be done by performing Ginzburg-Landau (GL) analysis as shown in Suppl. Mat. C. There are two typical possibilities for $j = 1$ that m in Eq. 6 equals 0, or ± 1 . In the former case,

$$\Delta_{m=0}(\mathbf{k}) = \Delta(|k|) \sin \theta_k e^{i\phi_k}. \quad (9)$$

Different from the usual case of $\Delta(\mathbf{k}) \propto Y_{10}(\hat{\mathbf{k}})$ exhibiting a nodal line, Eq. (9) only possesses nodal points repelling each other lying at two ends of a diameter of S_+ . In realistic systems, the spherical symmetry of S_+ is broken into the point group symmetry. Since the pairing gap is suppressed around gap nodes, it is preferred that the gap nodes are located at the minima of local density of states on S_+ . In the lattice case, two nodes attract each other and merge into a double one. Without loss of generality, they can be located at the north or south pole as

$$\Delta(\mathbf{k}) = \begin{cases} \Delta(|k|) \cos^2 \frac{\theta_k}{2} & (m = 1), \\ \Delta(|k|) \sin^2 \frac{\theta_k}{2} e^{2i\phi_k} & (m = -1), \end{cases} \quad (10)$$

respectively. Again its nodal structure is quite different from the usual axial pairing proportional to the spherical harmonic function $\mathcal{Y}_{1\pm 1}(\hat{\mathbf{k}})$. The pairing structures of Eq. 9 and Eq. 10 in the representation of σ_z -basis have also been studied in the context of pairing with magnetic dipolar interactions⁵³.

The above monopole Cooper pairing can be generalized to Fermi surfaces carrying opposite Chern numbers $\pm C$ with $C \geq 2$. In these cases, the monopole charge enclosed by the pairing surface S_+ equals $q_p = C$. Again,

the lowest pairing symmetry channel is $j = |q_p|$, and the gap function $\Delta(\mathbf{k})$ is a holomorphic or anti-holomorphic function on the helical Fermi surfaces. The mean-field free energy favors single nodes, and nodes repel each other forming a vortex lattice configuration. The small values of $q = 4$ and 6 may be relevant for Fermi surfaces with Chern numbers $C = \pm 2$ and ± 3 , and there exist regular tetrahedral and octahedral configurations for nodal locations. The optimal configurations are determined by complicated energetic issues, in particular, the anisotropy of the density of states will play a role to pin these nodes.

In summary, we have studied the Cooper pairing structure between two Fermi surfaces carrying opposite Chern numbers $\pm C$. The Cooper pairs also carry a non-trivial Berry phase structure characterized by the monopole charge $q_p = C$ so that their phases cannot be globally well-defined on the Fermi surfaces. The gap function $\Delta(\mathbf{k})$ generically possesses nodes with the total vorticity $2q_p$. These nodes are also the W-M points of the Hamiltonian in the BdG formalism. The surface modes arise both from the Weyl band structure and the pairing: the former exist inside the band gap, while the latter appear inside the pairing gap on FS_\pm . They connect to each other and their connection pattern are determined by the chirality pattern of the W-M points. When rotational symmetry is present, the pairing symmetry is classified in terms of the monopole harmonic functions. The lowest pairing channel is $j = |q_p|$ purely determined by the symmetry rather than interaction, and the corresponding pairing functions are holomorphic or anti-holomorphic functions on the pairing surface.

We have also performed the partial-wave analysis to the pairing interactions as shown in Suppl. Mat. D to show how the non-trivial topology of FS_\pm transforms the ordinary partial-wave channels into those characterized by monopole harmonics starting with $j = |q_p|$. Another possibility of Cooper pairing in doped Weyl metals is the intra-Fermi surface pairing with non-zero center of mass momenta, whose pairing phase structure does not possess non-trivial Berry phase structure on FS_\pm . The competition between the inter- and intra-Fermi surface pairings are discussed in Suppl. Mat. E.

Acknowledgments Y.L. thanks the Princeton Center for Theoretical Science at Princeton University for support. F.D.M.H. was supported in part by the MRSEC program at Princeton Center for Complex Materials, grant NSF-DMR-1420541, and by the W. M. Keck Foundation.

¹ K. Klitzing, G. Dorda, and M. Pepper, Phys. Rev. Lett. **45**, 494 (1980).

² D. C. Tsui, H. L. Stormer, and A. C. Gossard, Phys. Rev. Lett. **48**, 1559 (1982).

³ D. J. Thouless, M. Kohmoto, M. P. Nightingale, and M. den Nijs, Phys. Rev. Lett. **49**, 405 (1982).

⁴ F. Haldane, Phys. Rev. Lett. **51**, 605 (1983).

⁵ J. E. Avron, R. Seiler, and B. Simon, Phys. Rev. Lett. **51**, 51 (1983).

⁶ Q. Niu, D. Thouless, and Y. Wu, Phys. Rev. B **31**, 3372 (1985).

⁷ M. Kohmoto, Ann. Phys. **160**, 343 (1985).

- ⁸ J. E. Avron, R. Seiler, and B. Simon, *Phys. Rev. Lett.* **65**, 2185 (1990).
- ⁹ F. D. M. Haldane, *Phys. Rev. Lett.* **61**, 2015 (1988).
- ¹⁰ R. Karplus and J. M. Luttinger, *Phys. Rev.* **95**, 1154 (1954).
- ¹¹ T. Jungwirth, Q. Niu, and A. H. MacDonald, *Phys. Rev. Lett.* **88**, 207208 (2002).
- ¹² M. Onoda and N. Nagaosa, *Journal of the Physical Society of Japan* **71**, 19 (2002), <http://dx.doi.org/10.1143/JPSJ.71.19>.
- ¹³ F. D. M. Haldane, *Phys. Rev. Lett.* **93**, 206602 (2004).
- ¹⁴ N. Nagaosa, J. Sinova, S. Onoda, A. H. MacDonald, and N. P. Ong, *Rev. Mod. Phys.* **82**, 1539 (2010).
- ¹⁵ R. Yu, W. Zhang, H.-J. Zhang, S.-C. Zhang, X. Dai, and Z. Fang, *Science* **329**, 61 (2010), <http://www.sciencemag.org/content/329/5987/61.full.pdf>.
- ¹⁶ C.-Z. Chang, J. Zhang, X. Feng, J. Shen, Z. Zhang, M. Guo, K. Li, Y. Ou, P. Wei, L.-L. Wang, Z.-Q. Ji, Y. Feng, S. Ji, X. Chen, J. Jia, X. Dai, Z. Fang, S.-C. Zhang, K. He, Y. Wang, L. Lu, X.-C. Ma, and Q.-K. Xue, *Science* **340**, 167 (2013), <http://www.sciencemag.org/content/340/6129/167.full.pdf>.
- ¹⁷ C. L. Kane and E. J. Mele, *Phys. Rev. Lett.* **95**, 226801 (2005).
- ¹⁸ C. L. Kane and E. J. Mele, *Phys. Rev. Lett.* **95**, 146802 (2005).
- ¹⁹ B. A. Bernevig and S. C. Zhang, *Phys. Rev. Lett.* **96**, 106802 (2006).
- ²⁰ B. A. Bernevig, T. L. Hughes, and S. C. Zhang, *Science* **314**, 1757 (2006).
- ²¹ L. Fu and C. L. Kane, *Phys. Rev. B* **76**, 045302 (2007).
- ²² L. Fu, C. L. Kane, and E. J. Mele, *Phys. Rev. Lett.* **98**, 106803 (2007).
- ²³ J. E. Moore and L. Balents, *Phys. Rev. B* **75**, 121306 (2007).
- ²⁴ X.-L. Qi, T. L. Hughes, and S.-C. Zhang, *Phys. Rev. B* **78**, 195424 (2008).
- ²⁵ R. Roy, *Phys. Rev. B* **79**, 195322 (2009).
- ²⁶ R. Roy, *New J. Phys.* **12**, 065009 (2010).
- ²⁷ M. Z. Hasan and C. L. Kane, *Rev. Mod. Phys.* **82**, 3045 (2010).
- ²⁸ X.-L. Qi and S.-C. Zhang, *Rev. Mod. Phys.* **83**, 1057 (2011).
- ²⁹ X. Wan, A. M. Turner, A. Vishwanath, and S. Y. Savrasov, *Phys. Rev. B* **83**, 205101 (2011).
- ³⁰ A. A. Burkov and L. Balents, *Phys. Rev. Lett.* **107**, 127205 (2011).
- ³¹ K.-Y. Yang, Y.-M. Lu, and Y. Ran, *Phys. Rev. B* **84**, 075129 (2011).
- ³² T. Meng and L. Balents, *Phys. Rev. B* **86**, 054504 (2012).
- ³³ G. Y. Cho, J. H. Bardarson, Y.-M. Lu, and J. E. Moore, *Phys. Rev. B* **86**, 214514 (2012).
- ³⁴ D. T. Son and B. Z. Spivak, *Phys. Rev. B* **88**, 104412 (2013).
- ³⁵ P. Hosur and X. Qi, *Comptes Rendus Physique* **14**, 857 (2013), [arXiv:1309.4464](https://arxiv.org/abs/1309.4464) [cond-mat.str-el].
- ³⁶ M. M. Vazifeh and M. Franz, *Phys. Rev. Lett.* **111**, 027201 (2013).
- ³⁷ R. Nandkishore, D. A. Huse, and S. L. Sondhi, *Phys. Rev. B* **89**, 245110 (2014).
- ³⁸ P. Hosur, X. Dai, Z. Fang, and X.-L. Qi, *Phys. Rev. B* **90**, 045130 (2014).
- ³⁹ A. C. Potter, I. Kimchi, and A. Vishwanath, *Nature communications* **5** (2014).
- ⁴⁰ F. Haldane, [arXiv:1401.0529](https://arxiv.org/abs/1401.0529) (2014).
- ⁴¹ H. Wei, S.-P. Chao, and V. Aji, *Phys. Rev. B* **89**, 014506 (2014).
- ⁴² H. Weng, C. Fang, Z. Fang, B. A. Bernevig, and X. Dai, *Phys. Rev. X* **5**, 011029 (2015).
- ⁴³ A. A. Burkov, *Journal of Physics: Condensed Matter* **27**, 113201 (2015).
- ⁴⁴ S.-Y. Xu, C. Liu, S. K. Kushwaha, R. Sankar, J. W. Krizan, I. Belopolski, M. Neupane, G. Bian, N. Alidoust, T.-R. Chang, H.-T. Jeng, C.-Y. Huang, W.-F. Tsai, H. Lin, P. P. Shibayev, F.-C. Chou, R. J. Cava, and M. Zahid Hasan, *ArXiv e-prints*: 1501.01249 (2015), [arXiv:1501.01249](https://arxiv.org/abs/1501.01249) [cond-mat.mes-hall].
- ⁴⁵ S.-Y. Xu, I. Belopolski, N. Alidoust, M. Neupane, C. Zhang, R. Sankar, S.-M. Huang, C.-C. Lee, G. Chang, B. Wang, G. Bian, H. Zheng, D. S. Sanchez, F. Chou, H. Lin, S. Jia, and M. Zahid Hasan, *ArXiv e-prints*: 1502.03807 (2015), [arXiv:1502.03807](https://arxiv.org/abs/1502.03807) [cond-mat.mes-hall].
- ⁴⁶ B. Q. Lv, H. M. Weng, B. B. Fu, X. P. Wang, H. Miao, J. Ma, P. Richard, X. C. Huang, L. X. Zhao, G. F. Chen, Z. Fang, X. Dai, T. Qian, and H. Ding, *ArXiv e-prints*: 1502.04684 (2015), [arXiv:1502.04684](https://arxiv.org/abs/1502.04684) [cond-mat.mtrl-sci].
- ⁴⁷ B. Q. Lv, N. Xu, H. M. Weng, J. Z. Ma, P. Richard, X. C. Huang, L. X. Zhao, G. F. Chen, C. Matt, F. Bisti, V. Stokov, J. Mesot, Z. Fang, X. Dai, T. Qian, M. Shi, and H. Ding, *ArXiv e-prints*: 1503.09188 (2015), [arXiv:1503.09188](https://arxiv.org/abs/1503.09188) [cond-mat.mtrl-sci].
- ⁴⁸ G. Bednik, A. A. Zyuzin, and A. A. Burkov, *ArXiv e-prints*: 1506.05109 (2015), [arXiv:1506.05109](https://arxiv.org/abs/1506.05109) [cond-mat.str-el].
- ⁴⁹ S.-K. Jian, Y.-F. Jiang, and H. Yao, *Phys. Rev. Lett.* **114**, 237001 (2015).
- ⁵⁰ P. Hosur, *Phys. Rev. B* **86**, 195102 (2012).
- ⁵¹ T. T. Wu and C. N. Yang, *Nuclear Physics B* **107**, 365 (1976).
- ⁵² T. T. Wu and C. N. Yang, *Phys. Rev. D* **16**, 1018 (1977).
- ⁵³ Y. Li and C. Wu, *Scientific reports* **2** (2012).
- ⁵⁴ A. Larkin and Y. N. Ovchinnikov, *Zh. Eksperim. i Teor. Fiz.* **47** (1964).
- ⁵⁵ P. Fulde and R. A. Ferrell, *Phys. Rev.* **135**, A550 (1964).
- ⁵⁶ X.-L. Qi, T. L. Hughes, and S.-C. Zhang, *Phys. Rev. B* **81**, 134508 (2010).

Supplemental Materials

A. Lattice construction of the Weyl metal model

The Weyl metal model Eq. 4 studied in the main text can be formulated in the real space in a bipartite lattice with spinless fermions⁴⁰. After a partial Fourier transformation over the y and z -directions, the band Hamiltonian along the x -axis becomes

$$H_{k_y, k_z}^K = V_{k_y} \sum_i \left\{ c_{k_y, k_z}^{A, \dagger}(i) c_{k_y, k_z}^A(i) - c_{k_y, k_z}^{B, \dagger}(i) c_{k_y, k_z}^B(i) \right\} + \sum_i \left\{ t_+(k_y, k_z) c_{k_y, k_z}^{B, \dagger}(i) c_{k_y, k_z}^A(i+1) + t_- c_{k_y, k_z}^{A, \dagger}(i) c_{k_y, k_z}^B(i) + h.c. \right\}, \quad (11)$$

in which i is the index of unit cells containing A and B sites, $V_{k_y} = 2k_y$, $t_+(k_y, k_z) = -(k_y^2 + k_z^2)$ and $t_- = 1$. H^K is invariant under the inversion transformation with respect to the center of a bond along x -direction, *i.e.*, $A \leftrightarrow B$, $k_{y,z} \rightarrow -k_{y,z}$, and it breaks TR symmetry. This Hamiltonian gives rise to a pair of Weyl point located at $\pm \mathbf{K}_0 = (0, 0, \pm 1)$, respectively. For chemical potential $\mu > 0$, FS $_{\pm}$ enclosing $\pm \mathbf{K}_0$ possess the Chern number $C = \pm 1$, respectively. Consider the following pairing structure

$$H_{k_y, k_z}^{\Delta} = \sum_{i, a=A, B} \left\{ \Delta_x c_{k_y, k_z}^{a, \dagger}(i) c_{-k_y, -k_z}^a(i+1) + h.c. \right\} + \sum_i \left\{ 2i \Delta_y \sin k_y c_{k_y, k_z}^{A, \dagger}(i) c_{-k_y, -k_z}^B(i) + h.c. \right\}. \quad (12)$$

After projection to FS $_{+}$, the gap function $\Delta(\mathbf{k})$ exhibits two nodes at the north and south poles, respectively.

B. Monopole harmonic functions

In this section, we present the definition and basic properties of monopole harmonic functions. For convenience, we will formulate mostly in real space, and their momentum version can be obtained by replacing \hat{r} with $\hat{\mathbf{k}}$.

Consider a magnetic monopole located at the origin. For convenience, we choose the following gauge to describe its vector potential \mathbf{A} as

$$\mathbf{A}(\mathbf{r}) = \frac{g}{r} \frac{\hat{\mathbf{z}} \times \mathbf{r}}{|\mathbf{r}| + \mathbf{r} \cdot \hat{\mathbf{z}}} = \frac{g}{r} \tan \frac{\theta}{2} \hat{\phi}, \quad (13)$$

which is singular along the Dirac string from the origin to the south pole. The mechanical angular momentum is defined as $\mathbf{\Lambda} = \mathbf{r} \times (\mathbf{p} - \frac{e}{c} \mathbf{A})$, but $\mathbf{\Lambda}$ does not satisfy the commutation of the SU(2) algebra. The angular momentum satisfying the SU(2) algebra is define as

$$\mathbf{L} = \mathbf{\Lambda} - q\hat{r}, \quad (14)$$

where $\hat{q} = \frac{eg}{c\hbar}$. \mathbf{q} is a positive integer, or, half-integer, taking values of $\frac{1}{2}, 1, \frac{3}{2}, 2, \dots$. Because $\mathbf{\Lambda} \perp \mathbf{r}$, we can verify that

$$\Lambda^2 = L^2 - \hbar^2 q^2, \quad (15)$$

which is an operator identity. If an electron is confined on a sphere with radius R with a monopole of charge q located in the center of the sphere, its Hamiltonian can be described as

$$H = \frac{\hbar^2}{2mR^2} \Lambda^2 \quad (16)$$

The components of $L_{\pm} = L_x \pm iL_y$ and L_z are

$$L_z = -i\hbar \frac{\partial}{\partial \phi} - \hbar q$$

$$L_{\pm} = \hbar e^{\pm i\phi} \left(\pm \frac{\partial}{\partial \theta} + i \cot \theta \frac{\partial}{\partial \phi} - q \tan \frac{\theta}{2} \right), \quad (17)$$

L^2 is expressed as

$$\frac{L^2}{\hbar^2} = \frac{-1}{\sin^2 \theta} (\sin \theta \frac{\partial}{\partial \theta} (\sin \theta \frac{\partial}{\partial \theta} + \frac{1}{\sin^2 \theta} (i \frac{\partial}{\partial \phi} + q(1 - \cos \theta))^2 + \hbar^2 q^2). \quad (18)$$

The monopole harmonic functions $\mathcal{Y}_{q;jj_z}(\theta, \phi)$ are defined as

$$L^2 \mathcal{Y}_{q;jj_z}(\theta, \phi) = j(j+1) \hbar^2 \mathcal{Y}_{q;jj_z}(\theta, \phi)$$

$$L_z \mathcal{Y}_{q;jj_z}(\theta, \phi) = j_z \hbar \mathcal{Y}_{q;jj_z}(\theta, \phi), \quad (19)$$

where $j = |q|, |q| + 1, \dots$, and $j_z = -j, -j + 1, \dots, j$. There is a nice relation between the monopole harmonic functions and the rotation D -matrix as

$$\mathcal{Y}_{q;jm}(\theta, \phi) = \sqrt{\frac{2j+1}{4\pi}} \left[D_{m, -q}^j(\phi, \theta, -\phi) \right]^*$$

$$= \sqrt{\frac{2j+1}{4\pi}} e^{i(m+q)\phi} d_{m, -q}^j(\theta) \quad (20)$$

where $D_{m, m'}^j(\alpha, \beta, \gamma)$ is defined in the standard way as

$$D_{m, m'}^j(\alpha, \beta, \gamma) = \langle jm | e^{-iJ_z \alpha} e^{-iJ_y \beta} e^{-iJ_z \gamma} | jm' \rangle$$

$$= e^{-im\alpha - im'\gamma} d_{m, m'}^j(\beta), \quad (21)$$

and $d_{m, m'}^j(\beta) = \langle jm | e^{-iJ_y \beta} | jm' \rangle$. The expression for $d_{m, m'}^j(\beta)$ is

$$d_{m, m'}^j(\beta) = \sqrt{\frac{(j+m')!(j-m)!}{(j+m)!(j-m)!}} \left(\cos \frac{\beta}{2} \right)^{m'+m}$$

$$\times \left(\sin \frac{\beta}{2} \right)^{m'-m} P_{j-m'}^{m'-m, m'+m}(\cos \beta), \quad (22)$$

where the Jacobi polynomial $P_{j-m'}^{m'-m, m'+m}(\cos \beta)$ follows the definition as

$$P_n^{a, b}(x) = \frac{(-)^n}{2^n n!} (1-x)^{-a} (1+x)^{-b}$$

$$\times \frac{d^n}{dx^n} [(1-x)^{a+n} (1+x)^{b+n}]. \quad (23)$$

It will also be useful to introduce the two-component spinor notation $u = \cos \frac{\theta}{2}, v = \sin \frac{\theta}{2} e^{i\phi}$. In this notation, the expression of $\mathcal{Y}_{-q;j=q,j_z}(\theta, \phi)$ is simple in which $q > 0$ as

$$\mathcal{Y}_{-q;j=q,m}(\theta, \phi) = \left\{ \frac{2q+1}{4\pi} \binom{2q}{q-m} \right\}^{\frac{1}{2}} u^{q+m} v^{*,q-m}. \quad (24)$$

The relation between $\mathcal{Y}_{q;jm}(\theta, \phi)$ and $\mathcal{Y}_{-q;jm}(\theta, \phi)$ is

$$\mathcal{Y}_{q;jm}(\theta, \phi) = (-)^{q+m} \mathcal{Y}_{-q;j-m}^*(\theta, \phi).$$

For the purpose of the main body article, we will use monopole harmonic functions defined in momentum space. To maintain the SU(2) algebra, the angular momentum operator \mathbf{L} in the presence of the monopole is augmented to

$$\mathbf{L} = \hbar \mathbf{k} \times \left(-i\partial_{\mathbf{k}} - \frac{1}{k} \mathbf{A}(\mathbf{k}) \right) - q\hbar \hat{\mathbf{k}}, \quad (25)$$

and the vector potential under the gauge chosen above is $\mathbf{A}(\mathbf{k}) = q \tan \frac{\theta_k}{2} \hat{e}_{\phi_k}$. We can simply replace polar and azimuthal angles of θ and ϕ of \hat{r} with that of \hat{q} in the expressions above to yield $\mathcal{Y}_{q;jm}(\hat{\mathbf{k}})$. Again for $\mathcal{Y}_{q;jm}(\hat{\mathbf{k}})$, j starts with $|q|$ and takes values of $|q|, |q| + 1, \dots$. For the lowest value $j = |q|$, $\mathcal{Y}_{q;j=|q|,m}(\hat{\mathbf{k}})$'s are holomorphic (anti-holomorphic) functions on the unit sphere for $q < 0$ ($q > 0$).

C. Ginzburg-Landau analysis

To analyze the possible pairing configuration with $j = |q_p| = 1$, we perform the GL free energy analysis. The GL free energy is constructed as

$$F_G = \alpha |\Delta|^2 + \beta_1 |\Delta|^4 + \beta_2 |\Delta|^4 \sum_{mm'} c_{1m}^* c_{1,-m}^* c_{1m'} c_{1,-m'},$$

in which $|\Delta|$ is the magnitude of gap and the normalized coefficients c_{1m} defined in Eq. (6) control the angular distribution of the gap function. Without loss of generality, F_{GL} is minimized when c_{1m} 's take the component of $m = 1$ or $m = -1$ at $\beta_2 > 0$ and of $m = 0$ at $\beta_2 < 0$, respectively. Applying rotations to these configurations generates other equivalent pairing configurations. Following the standard terminology, we denote the former cases of $m = \pm 1$ and the latter one of $m = 0$ as the axial and the polar pairing, respectively.

The Bogoliubov quasi-particle spectra become

$$E(\mathbf{k}) = \sqrt{\epsilon_k^2 + \Delta^2 (|k|) |f(u_k, v_k)|^2}. \quad (26)$$

Assuming a fixed magnitude $\Delta(|k|)$ and normalized $f(\hat{\mathbf{k}})$, the free energy functional depends on the location of nodes through the relation of $F[u_k, v_k] = -\frac{2}{\beta} \sum_{\mathbf{k}} \ln(2 \cosh \beta E(\mathbf{k}))$. Different from the vortex problem in real space, $F[u_k, v_k]$ does not depend on the phase

gradient in momentum space but only on the magnitude distribution of $\Delta(\mathbf{k})$. Because of the convexity of F , the two nodes repel each other on S_+ , and in the optimal configuration they lie at two ends of a diameter, say, the north and south poles. In other words, the mean-field results give rise to $\beta_2 < 0$, and the corresponding pairing is polar with $m = 0$. Nevertheless, that case of $\beta_2 > 0$ cannot be ruled out. The consequential axial pairing with $m = \pm 1$ will result beyond the mean-field theory arising from strong correlation effect.

D. Partial-wave analysis of interactions by monopole harmonics

In this section, we elaborate the pair scattering interactions. Since the inter-Fermi surface Cooper pairing is between two electrons with parallel spins for the FS $_{\pm}$, we only consider the triplet channel pairing whose Hamiltonian is expressed as

$$H_{pair} = \frac{1}{V_0} \sum_{\mathbf{k}, \mathbf{k}'; m} V_t(\mathbf{k}, \mathbf{k}') \chi_{1m}^{\dagger}(\mathbf{k}) \chi_{1m}(\mathbf{k}') + h.c., \quad (27)$$

in which V_0 is the system volume; $\chi_{1m}^{\dagger}(\mathbf{k}) = \sum_{\sigma\sigma'} \langle 1m | \frac{1}{2}\sigma; \frac{1}{2}\sigma' \rangle c_{\sigma}^{\dagger}(\mathbf{K}_0 + \mathbf{k}) c_{\sigma'}^{\dagger}(-\mathbf{K}_0 - \mathbf{k})$ are the spin triplet pairing operator. Because usual interactions in solids do not directly flip electron spins, the spin index m in Eq. (27) is expressed in the S_z -eigenbasis. Eq. (27) is not expressed in the helical basis, and hence it is still not the low energy pairing Hamiltonian in accommodation to the helical Fermi surfaces yet. After projecting the pairing Hamiltonian Eq. (27) into the helical Fermi surface, we arrive at

$$\tilde{H}_{pair} = \sum_{\mathbf{k}, \mathbf{k}'} \tilde{V}(\mathbf{k}, \mathbf{k}') P^{\dagger}(\mathbf{k}) P(\mathbf{k}') + h.c., \quad (28)$$

in which $\tilde{V}(\mathbf{k}, \mathbf{k}') = \langle P(\mathbf{k}') | H_{pair} | P(\mathbf{k}) \rangle$ is the projected pair scattering matrix element. It can be expressed as

$$\tilde{V}(\mathbf{k}, \mathbf{k}') = \frac{4\pi}{3} \mathcal{Y}_{-1;1m}^*(\hat{k}) V_t(\mathbf{k}, \mathbf{k}') \mathcal{Y}_{-1;1m}(\hat{k}'). \quad (29)$$

Here, $P(\mathbf{k}) = \sum_{m=-1}^1 \sqrt{\frac{4\pi}{3}} \mathcal{Y}_{-1;1m}(\hat{\mathbf{k}}) \chi_{1m}(\mathbf{k})$ was used and the rotational invariance of the interaction was assumed. $\Delta(\mathbf{k})$ is the gap function determined by the self-consistent equation

$$\Delta(\mathbf{k}) = \frac{1}{V_0} \sum_{\mathbf{k}'} \tilde{V}(\mathbf{k}, \mathbf{k}') \langle P(\mathbf{k}') \rangle. \quad (30)$$

Because of fermion statistics, the pair scattering matrix element in Eq. (27) is expressed as

$$V_t(\mathbf{k}, \mathbf{k}') = V(\mathbf{k} - \mathbf{k}') - V(\mathbf{k} + \mathbf{k}' + 2\mathbf{K}_0), \quad (31)$$

in which the first and second terms are the intra and inter-Fermi surface scattering, respectively. If we neglect the inter-Fermi surface scattering which involves large

momentum transfer, $V_t(\mathbf{k}, \mathbf{k}')$ can be assumed only depending on the relative angle between \mathbf{k} and \mathbf{k}' , i.e., $V_t(\mathbf{k}, \mathbf{k}') = V_t(\hat{k} \cdot \hat{k}')$. Unlike the usual case, i.e., $\mathbf{K}_0 = 0$, that V_t only contains the odd partial-wave channels, here, both even and odd partial-wave channels are allowed as $V(\hat{k} \cdot \hat{k}') = \sum_{lm} 4\pi g_l Y_{lm}^*(\hat{k}) Y_{lm}(\hat{k}')$ in which $l = 0, 1, 2, \dots$. As will be proved below, after the projection defined in Eq. (29), the pairing interaction becomes

$$\tilde{V}(\hat{k} \cdot \hat{k}') = \sum_{jm} \tilde{g}_j \mathcal{Y}_{-1, jm}^*(\hat{k}') \mathcal{Y}_{1, jm}(\hat{k}), \quad (32)$$

in which

$$\tilde{g}_j = \frac{1}{2j+1} \sum_{l=j, j\pm 1} (2l+1) g_l |\langle l0; 11 | j1 \rangle|^2, \quad (33)$$

and the partial wave channels start with $j = 1$. In other words, the projection to the helical Fermi surfaces reorganize the partial-wave channels, and thus promoted the lowest partial wave channel from $j = 0$ to $j = 1$. The actual pairing channel that the system takes is determined by the most negative pairing matrix eigenvalue $V_{j'}$.

Below, we prove Eq. (32). Starting from Eq. (29), since V_t can be decomposed by usual spherical harmonics, we have

$$\tilde{V}(\hat{k} \cdot \hat{k}') = -\frac{(4\pi)^2}{3} \sum_{m_1} \mathcal{Y}_{-1; 1m_1}^*(\hat{k}) \mathcal{Y}_{-1; 1m_1}(\hat{k}') \left[\sum_{l_2 m_2} g_{l_2} Y_{l_2 m_2}^*(\hat{k}) Y_{l_2 m_2}(\hat{k}') \right]. \quad (34)$$

where g_{l_2} is the interaction strength of V_t in the l_2 -th partial-wave channel. To further simplify $\tilde{V}(\hat{k} \cdot \hat{k}')$, the composition of monopole harmonics^{51,52} will be employed, which can be derived by using D-matrices as follows: Let us start from the composition known for irreducible tensors of angular momentum,

$$\Phi_{l_1 l_2 l_3 m_3} = \sum_{m_1 m_2} \Phi_{l_1 m_1} \Phi_{l_2 m_2} \langle l_3, m_3 | l_1, m_1; l_2, m_2 \rangle, \quad (35)$$

Alternatively,

$$\Phi_{l_1 m_1} \Phi_{l_2 m_2} = \sum_{l_3 m_3} \Phi_{l_1 l_2 l_3 m_3} \langle l_3, m_3 | l_1, m_1; l_2, m_2 \rangle \quad (36)$$

Applying a rotation to both sides of Eq. (36), we have

$$D(g) \Phi_{l_1 m_1} \Phi_{l_2 m_2} = \sum_{l_3 m_3} D(g) \Phi_{l_1 l_2 l_3 m_3} \langle l_3, m_3 | l_1, m_1; l_2, m_2 \rangle. \quad (37)$$

It can be represented by D-matrices as

$$\sum_{m'_1 m'_2} \Phi_{l_1 m'_1} \Phi_{l_2 m'_2} D_{m'_1, m_1}^{l_1}(g) D_{m'_2, m_2}^{l_2}(g) = \sum_{l_3 m_3 m'_3} \Phi_{l_1 l_2 l_3 m'_3} D_{m'_3, m_3}^{l_3}(g) \langle l_3, m_3 | l_1, m_1; l_2, m_2 \rangle, \quad (38)$$

Using Eq. (35), the right hand side of the above equation becomes

$$\sum_{l_3 m_3 m'_3} \sum_{m'_1 m'_2} \Phi_{l_1 m'_1} \Phi_{l_2 m'_2} D_{m'_3, m_3}^{l_3}(g) \langle l_3, m'_3 | l_1, m'_1; l_2, m'_2 \rangle \langle l_3, m_3 | l_1, m_1; l_2, m_2 \rangle. \quad (39)$$

Therefore, the composition rule of D-matrices is obtained as

$$D_{m'_1, m_1}^{l_1}(g) D_{m'_2, m_2}^{l_2}(g) = \sum_{l_3 m_3 m'_3} \langle l_3, m'_3 | l_1, m'_1; l_2, m'_2 \rangle \langle l_3, m_3 | l_1, m_1; l_2, m_2 \rangle D_{m'_3, m_3}^{l_3}(g). \quad (40)$$

By changing variables, we have

$$D_{m_1, -q_1}^{l_1*}(g) D_{m_2, -q_2}^{l_2*}(g) = \sum_{l_3 = |l_1 - l_2|}^{l_1 + l_2} \langle l_3, m_3 | l_1, m_1; l_2, m_2 \rangle \langle l_3, -q_3 | l_1, -q_1; l_2, -q_2 \rangle D_{m_3, -q_3}^{l_3*}(g), \quad (41)$$

where $m_3 = m_1 + m_2$, $q_3 = q_1 + q_2$. Using Eq. (20), the composition of monopole harmonics can be derived from the above composition of D-matrices as

$$\sqrt{\frac{4\pi}{2l_1+1}} \sqrt{\frac{4\pi}{2l_2+1}} \mathcal{Y}_{q_1; l_1 m_1}(\hat{k}) \mathcal{Y}_{q_2; l_2 m_2}(\hat{k}) = \sum_{l_3} \langle l_3, m_3 | l_1, m_1; l_2, m_2 \rangle \langle l_3, -q_3 | l_1, -q_1; l_2, -q_2 \rangle \sqrt{\frac{4\pi}{2l_3+1}} \mathcal{Y}_{q_3; l_3 m_3}(\hat{k}). \quad (42)$$

For our derivation, let us take a special case of $q_1 = -1$, $q_2 = 0$, and $l_1 = 1$,

$$\mathcal{Y}_{-1;1m_1}(\hat{k})Y_{l_2m_2}(\hat{k}) = \sum_{l_3=l_2-1}^{l_2+1} \sqrt{\frac{3(2l_2+1)}{4\pi(2l_3+1)}} \langle l_3, m_3 | 1, m_1; l_2, m_2 \rangle \langle l_3, 1 | 1, 1; l_2, 0 \rangle \mathcal{Y}_{-1;l_3m_3}(\hat{k}). \quad (43)$$

Then, Eq. (34) can be simplified as

$$\begin{aligned} \tilde{V}(\hat{k} \cdot \hat{k}') &= -4\pi \sum_{l_2} g_{l_2} \sum_{m_1, m_2} \sum_{l_3=l_2-1}^{l_2+1} \sum_{l'_3=l_2-1}^{l_2+1} \frac{2l_2+1}{\sqrt{(2l_3+1)(2l'_3+1)}} \times \\ &\quad \times \langle l_3, m_3 | 1, m_1; l_2, m_2 \rangle \langle l_3, 1 | 1, 1; l_2, 0 \rangle \mathcal{Y}_{-1;l_3m_3}^*(\hat{k}) \times \\ &\quad \times \langle l'_3, m_3 | 1, m_1; l_2, m_2 \rangle \langle l'_3, 1 | 1, 1; l_2, 0 \rangle \mathcal{Y}_{-1;l'_3m_3}(\hat{k}'). \end{aligned} \quad (44)$$

The orthogonality of Clebsch-Gordan coefficients $\sum_{m_2} \langle l_3, m_3 | 1, m_3 - m_2; l_2, m_2 \rangle \langle l'_3, m_3 | 1, m_3 - m_2; l_2, m_2 \rangle = \delta_{l_3 l'_3}$ further gives

$$\begin{aligned} \tilde{V}(\hat{k} \cdot \hat{k}') &= -4\pi \sum_{l_2} g_{l_2} \sum_{l_3=l_2-1}^{l_2+1} \frac{2l_2+1}{2l_3+1} \langle l_3, 1 | 1, 1; l_2, 0 \rangle^2 \sum_{m_3} \mathcal{Y}_{-1;l_3m_3}^*(\hat{k}) \mathcal{Y}_{-1;l_3m_3}(\hat{k}') \\ &= -4\pi \sum_{l_3 m_3} \tilde{g}_{l_3} \mathcal{Y}_{-1;l_3 m_3}^*(\hat{k}) \mathcal{Y}_{-1;l_3 m_3}(\hat{k}'). \end{aligned} \quad (45)$$

where $\tilde{g}_{l_3} = \frac{1}{2l_3+1} \sum_{l_2=l_3-1}^{l_3+1} (2l_2+1) g_{l_2} \langle l_3, 1 | 1, 1; l_2, 0 \rangle^2$ as shown in Eq. (32) of the main text.

E. Intra-Fermi surface pairing

Another pairing possibility is the intra Fermi surface pairing: Cooper pairings take place within each Fermi surface FS_{\pm} carrying finite momentum $\pm K_0$, respectively, thus this is an example of the Fulde-Ferrel-Larkin-Ovchinnikov type pairing^{54,55}. The intra FS_{\pm} pairing operators are defined as

$$P_{\pm}^{\dagger}(\mathbf{k}) = \alpha_{\pm}^{\dagger}(\mathbf{k}) \alpha_{\pm}^{\dagger}(-\mathbf{k}), \quad P_{\pm}^{\dagger}(\mathbf{k}) = \alpha_{\pm}^{\dagger}(\mathbf{k}) \alpha_{\pm}^{\dagger}(-\mathbf{k}) \quad (46)$$

which satisfy $[\mathbf{S} \cdot \hat{\mathbf{k}}, P_{\pm}^{\dagger}(\mathbf{k})] = 0$. Therefore, their pairing phases can be well-defined globally over the sphere $|k| = k_f$ without non-trivial monopole structure, such that the gap functions can be decomposed into the usual spherical harmonic functions as $\Delta_{\pm}(\mathbf{k}) = \Delta_{jm}(|k|) \sum_{j m} c_{\pm, jm} \mathcal{Y}_{jm}(\hat{\mathbf{k}})$. In the simplest case with $j = m = 0$, the pairing $\Delta_{0, \pm}$ is a mixture between the conventional s -wave and $^3\text{He-B}$ type p -wave pairings. Under the σ_z -eigen basis, they are written as

$$P_{\pm}(\mathbf{k}) \propto \chi_{\pm;00}^{\dagger}(\mathbf{k}) \pm \mathbf{k} \cdot \chi_{\pm}(\mathbf{k}), \quad (47)$$

in which the singlet and triplet pairing operators are $\chi_{\pm;00}^{\dagger}(\mathbf{k}) = \sum_{\alpha\beta} \langle 00 | \frac{1}{2} \alpha \frac{1}{2} \beta \rangle c_{\alpha}^{\dagger}(\pm K_0 + \mathbf{k}) c_{\beta}^{\dagger}(\pm K_0 - \mathbf{k})$, and

$\chi_{\pm}(\mathbf{k}) = c_{\alpha}^{\dagger}(\pm K_0 + \mathbf{k}) i(\sigma_y \sigma)_{\alpha\beta} c_{\beta}^{\dagger}(\pm K_0 - \mathbf{k})$. This pairing is fully gapped, and thus can be characterized by the integer-valued topological index in the DIII class for 3D superconductivity. According to the criterion in Ref. [56], the overall pairing structure is topologically non-trivial according to $\Delta_{+} = \mp \Delta_{-}$, respectively.

The competition between the inter- and intra-Fermi surface pairing is an interesting question depending on the concrete pairing mechanism. The inter-Fermi surface pairing is spin-triplet, while the intra-Fermi surface one is a mixture between spin singlet and triplet. Thus, if the pairing mechanism is dominated by strong correlation effects such as magnetic fluctuations, the inter-Fermi surface pairing could be more favorable. On the other hand, because of the lattice effect, FS_{\pm} generically are not symmetric with respect to $\mp K_0$, and thus, $\mathbf{K}_0 \pm \mathbf{k}$ could not both at Fermi surfaces and so do $-\mathbf{K}_0 \pm \mathbf{k}$. This asymmetry suppresses the intra-Fermi surface pairing but does not affect the inter-Fermi surface pairing. In this case, the inter-Fermi surface pairing is more favorable.